

Influence of the floating potential on micro-hollow cathode operation

D. Levko,¹ Y. P. Bliokh,² and Ya. E. Krasik²

¹*Department of Aerospace Engineering and Engineering Mechanics, The University of Texas at Austin, Austin, Texas 78712, USA*

²*Department of Physics, Technion, 32000 Haifa, Israel*

(Received 7 March 2015; accepted 20 May 2015; published online 3 June 2015)

The influence of a keeper electrode with a floating potential on the operation of a micro-hollow cathode is studied using the two-dimensional particle-in-cell Monte Carlo collisions model. The floating potential is determined self-consistently, taking into account the electron and ion charges collected by the keeper and the potential induced by the plasma non-compensated space charge. It is shown that the parameters of the micro-hollow cathode operation vary significantly, according to whether the keeper potential is floating or has a specified constant value. © 2015 AIP Publishing LLC.

[<http://dx.doi.org/10.1063/1.4922070>]

I. INTRODUCTION

Currently, ion and Hall plasma thrusters are used as engines to provide the electric propulsion for the correction of satellite orbits and for long-term space missions.¹ The thrust in these engines is generated by the flux of accelerated ions. The electron beam produced by a hollow cathode (HC) is used for gas ionization inside the thrusters and for space-charge neutralization of the extracted ion beam in order to preserve a zero net charge leaving the thruster. Most of the HCs that are presently used in electric propulsion are driven by the thermionic electron emission from emitters heated up to temperatures exceeding 1000 K and having a work function in the range of 1.3–2.5 eV.^{1–6} At the beginning of the HC operation, an external heater is used to heat the emitter to a temperature sufficient for thermionic emission of electrons, which produce the plasma inside the HC. This plasma supplies ions that are accelerated toward the emitter, mainly inside the sheath formed between the plasma and emitter. In the steady state operation of the HC, the energy delivered by these ions serves as a main heat source maintaining the emitter temperature at the desired level. However, the interaction of these ions with different parts of the HC can cause their sputtering, which finally leads to the HC failure and, accordingly, limits the lifetime of the thruster.

In the design of the common HC, the emitter is enclosed in a cylinder having an orifice with a diameter smaller than the internal diameter of the emitter. This cylinder in its turn is placed coaxially inside a so-called keeper, which is kept at a floating potential during the steady state operation of the HC.^{1,4} The main purposes of the keeper are to facilitate the turning on of the HC discharge, maintain the cathode temperature, and protect the emitter from the interaction of relatively high-energy ions that might limit the HC lifetime.¹ These high-energy ions (up to several tens of eV) are generated in the gap between the keeper and anode. The keeper lifetime is a crucial issue for the long-term operation of the thruster.

The HC electron current that is required for gas ionization inside the ion engine and neutralization of the ion beam determines the parameters of the HC (dimensions, gas flow

rate, emitter potential, etc.). In electrical micro-propulsion,⁷ low power consumption HCs with mm and sub-mm scale dimensions of the emitter and orifice are used.^{4,6–9}

In the most commonly used HC, the keeper potential is floating. Currently, two main approaches are used for modeling the HC plasma discharge when the potential of the keeper is floating. The first approach⁸ considers the value of the floating potential that was obtained in experiments; in simulations, this potential is kept constant. The second self-consistent approach is described in Ref. 3. This approach is based on taking account of the ion and electron currents toward the keeper, which allows the keeper potential (both floating and biased) to be calculated by using an iteration method solving the sheath equation with appropriate boundary conditions.

In micro-hollow cathodes (micro-HC), the characteristic dimensions of which are comparable to or even smaller than the electron mean free-path, the plasma electrons are, strictly speaking, far from thermal equilibrium. This raises questions about the application of sheath models for determining the ion and electron fluxes on the keeper surface and, accordingly, the calculation of the keeper floating potential.

In the present paper, a self-consistent method for calculating the keeper floating potential in the Particle-in-Cell (PIC) model of the micro-HC is proposed. This method is implemented in the two-dimensional PIC Monte Carlo collisions (2D PIC/MCC) model and applied for studying the influence of the keeper's floating potential on the micro-HC operation.

II. NUMERICAL MODEL

The 2D PIC/MCC model that is used in the present study was described in detail in earlier publications.⁵ The model is based on the 2D Cartesian module of the open-source WARP PIC code.¹⁰ The plasma consists of electrons, ions Xe^+ , and neutral Xe atoms. For simplicity, the distribution of the neutral gas density is assumed uniform and constant in time, and the temperature of the Xe gas is equal to that of the emitter. Here, let us note that, in general, the assumption of uniform neutral gas density is not

valid for the HCs that are used for electric propulsion applications,¹ and it is understood that non-uniform distribution of neutral density significantly influences the micro-HC operation¹¹ and changes the value of the keeper floating potential as well.

The 2D simulation domain is shown in Fig. 1. This geometry corresponds to the parameters of the experiments described in Ref. 4. The domain consists of three coaxial electrodes, namely, a hollow emitter (electrode #0), anode (#1), and keeper (#2). Here, let us note that the design of HCs commonly includes a cathode orifice, which significantly influences the life-time of the emitter. However, in the present study of the self-consistent calculation of the keeper floating potential, this part of the HC was omitted for simplicity. The electrons are emitted from the inner surface of the emitter because of the thermionic emission. The latter is described by the Richardson-Dushman equation.¹

In addition, the secondary electron emission from the emitter due to ion bombardment is considered in the model.¹² The energy of secondary emitted electrons is defined as $\varepsilon_e = \varepsilon_{ion} - 2\varphi$,¹² where ε_{ion} is the ionization threshold of Xe atoms (12.1 eV) and φ is the emitter work function. The latter is taken to be equal to 2.5 eV. The secondary electron emission coefficient is defined by the phenomenological expression $\gamma \approx 0.016 \cdot (\varepsilon_{ion} - 2\varphi) \approx 0.1$,¹² where the unit of the work function and the ionization threshold values is eV.

Two modes of the micro-HC operation are investigated in this study. In the first mode, the keeper's potential is kept constant, while in the second mode it is floating. In order to determine the keeper's floating potential, we extend the method described in Ref. 13 to the case where a non-compensated space charge is present in the system. Let us consider the system that consists of three electrodes: an emitter, keeper, and anode, as mentioned above. The electrodes' potentials V_i and charges Q_i are connected by the following system of equations:

$$\begin{aligned} Q_0 &= C_{01}(V_0 - V_1) + C_{02}(V_0 - V_2), \\ Q_1 &= C_{10}(V_1 - V_0) + C_{12}(V_1 - V_2), \\ Q_2 &= C_{20}(V_2 - V_0) + C_{21}(V_2 - V_1). \end{aligned} \quad (1)$$

Here, $C_{ik} = C_{ki}$ is the capacitance between electrodes “ i ” and “ k ”; indexes “0,” “1,” and “2” relate to the emitter, anode, and keeper electrodes, respectively. Introducing $C_{ii} = \sum_{k \neq i} C_{ik}$ (for instance, $C_{22} = C_{21} + C_{20}$), the system of equations (1) can be re-written in matrix form,

$$\begin{pmatrix} Q_0 \\ Q_1 \\ Q_2 \end{pmatrix} = \hat{C} \begin{pmatrix} V_0 \\ V_1 \\ V_2 \end{pmatrix}, \quad (2)$$

where \hat{C} is the matrix of capacitances

$$\hat{C} = \begin{vmatrix} C_{00} & -C_{01} & -C_{02} \\ -C_{10} & C_{11} & -C_{12} \\ -C_{20} & -C_{21} & C_{22} \end{vmatrix}. \quad (3)$$

For the HC case considered here, when the emitter and anode potentials are known values, i.e., $V_0 = U_0$ and $V_1 = 0$, one obtains for the keeper charge

$$Q_2 = -C_{20}U_0 + C_{22}V_2. \quad (4)$$

Following Ref. 13, capacitances C_{20} and C_{22} can be determined by the solution of the Laplace equation $\Delta\varphi^{(v)} = 0$ with the boundary conditions $V_0 = V_1 = 0$ and $V_2 = 1$ V ($Q_2 = C_{22}V_2 = C_{22}$). Then, using the Gauss law

$$\oint_{\Gamma} \frac{\partial\varphi^{(v)}}{\partial\vec{n}} d\vec{S} = -\frac{Q_2}{\varepsilon_0}. \quad (5)$$

The charge Q_2 can be calculated and, accordingly, the capacitance $C_{22} = Q_2/V_2$. Here, Γ denotes the surface integral, S the keeper electrode surface, and ε_0 the permittivity of free space. Similarly, taking the integral (5) around the cathode electrode, the charge $Q_0 = -C_{02}V_2$ is obtained and, accordingly, the capacitance $C_{02} = C_{20}$. Then, using Eq. (4), the floating keeper potential can be calculated with the determined capacitances C_{20} and C_{22}

$$V_2^{(v)} = \frac{1}{C_{22}} (Q_2^{(v)} + C_{20}U_0). \quad (6)$$

Here, $Q_2^{(v)}$ is the charge of the keeper in the case of a vacuum.

Now, for zero potential at the emitter, anode, keeper electrodes, and a known distribution of the plasma space charge $\rho(r)$, applying the Poisson equation, the potential distribution $\varphi^{(p)}(r)$ can be determined. Then, using this distribution $\varphi^{(p)}(r)$, the charge Q_2 that results in zero potential at the keeper electrode can be calculated.

The potential $\varphi(r) = \varphi^{(v)}(r) + \varphi^{(p)}(r)$ satisfies the Poisson equation with the given boundary conditions at the emitter and anode and the charge $Q = Q_2^{(v)} + Q_2^{(p)}$ at the keeper electrode, where the charge $Q_2^{(p)}$ is a known value. Here, let us note that the total charge Q is also defined by the

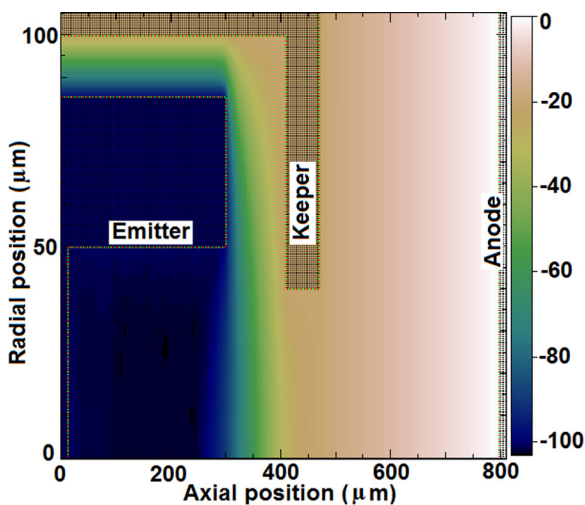


FIG. 1. Micro-HC geometry and the potential distribution without plasma formation.

charge of the plasma electrons and ions collected by the keeper. Thus, the unknown charge can be found as $Q_2^{(v)} = Q - Q_2^{(p)}$. Using this charge and Eq. (6), the floating potential is calculated as

$$V_2^{(v)} = V_{float} = \frac{1}{C_{22}} (Q_0 + Q - Q^{(p)} + C_{20}U_0). \quad (7)$$

Equation (7) also takes into account that the keeper potential can be kept constant during some initial time after the micro-HC is turned on by the introduction of charge Q_0 . This charge is found in the same manner as the surface integral around the keeper, at time τ when the keeper potential is turned on in the floating mode. The values of C_{22} and C_{20} are calculated once prior to the beginning of simulations. Then, at each time step, the charge Q collected by the keeper from the plasma is saved and the Poisson equation for zero potentials at all the electrodes is solved in order to define the charge $Q^{(p)}$ induced by the plasma on the keeper. This updates the value of the keeper potential, which is used as the boundary condition for the Poisson equation in the next time step. In such a manner, the floating potential is calculated self-consistently, allowing one to obtain the 2D distribution of the electric field that is used for pushing particles into new positions.

III. RESULTS AND DISCUSSION

2D PIC/MCC simulations were conducted for inner and outer emitter radii of $50 \mu\text{m}$ and $85 \mu\text{m}$, respectively, and an emitter length of $300 \mu\text{m}$; the keeper inner radius, length, and orifice radius were $100 \mu\text{m}$, $410 \mu\text{m}$, and $40 \mu\text{m}$, respectively, and the emitter-anode gap was $500 \mu\text{m}$ (see Fig. 1). The emitter potential of -100 V and temperature of 1600 K were kept constant. These parameters correspond to those of the micro-HC studied in Ref. 4.

The gas temperature was assumed equal to the emitter temperature for simplicity. A constant Xe gas density of $4.5 \times 10^{22} \text{ m}^{-3}$ (pressure of 10^3 Pa) is maintained. In the simulations, the keeper voltage was kept either constant and equal to -20 V or floating. In the latter case, the keeper floating potential was turned on with some time delay τ with respect to the beginning of the simulations. During time

$t < \tau$, the keeper potential was kept constant and equal to -20 V .

The time delay τ strongly depends on the gas pressure and keeper-anode gap. Namely, a decrease in the gas pressure or increase in the keeper-anode gap leads to an increase in the time necessary for the dense plasma to form outside the keeper. Therefore, one needs to increase the value of τ in order to obtain the micro-HC discharge with the floating keeper's potential (see discussion in Sec. III B).

A. Constant keeper potential

The results of the simulations for the constant keeper potential (-20 V) are shown in Figs. 2–4. One can see that the plasma formation is characterized by three main phases.

The first phase is characterized by an almost zero electric field inside the emitter and intense electron thermionic emission, mostly at the right edge of the emitter because of the enhanced electric field at that location. In the vicinity of the emitter, electrons form a negative space charge, which partially screens the emission [see Fig. 2(a)]. Electrons, which are emitted near the exit of the micro-HC, propagate toward the keeper, gaining energy in the electric field and ionizing the background gas [see Figs. 2(b) and 2(c)]. Some fraction of the electrons leaves the emitter-keeper gap through the keeper's orifice and generates dilute plasma inside the keeper-anode gap.

During the second phase (see Fig. 3), plasma with a typical density $n_e \sim 10^{20} \text{ m}^{-3}$ is formed inside the emitter-keeper gap and penetrates deep into the emitter. This plasma acquires a positive potential with respect to the emitter and changes drastically the potential distribution inside the emitter [see Fig. 3(a)]. A plasma sheath is formed near the cathode surface [see Figs. 2(b) and 3(b)]. The sheath potential exceeds the ionization potential of Xe atoms. Therefore, emitted electrons, which are accelerated in the sheath, acquire sufficient energy to generate the plasma inside the emitter.

The third steady-state phase of the micro-HC operation (see Fig. 4) is characterized by the formation of high-density plasma ($n_e \sim 10^{21} \text{ m}^{-3}$), which fills the entire emitter. The mean electron energy in the plasma bulk is $\sim 7.0 \text{ eV}$, which significantly exceeds the ion mean energy $\sim 0.5 \text{ eV}$. In this

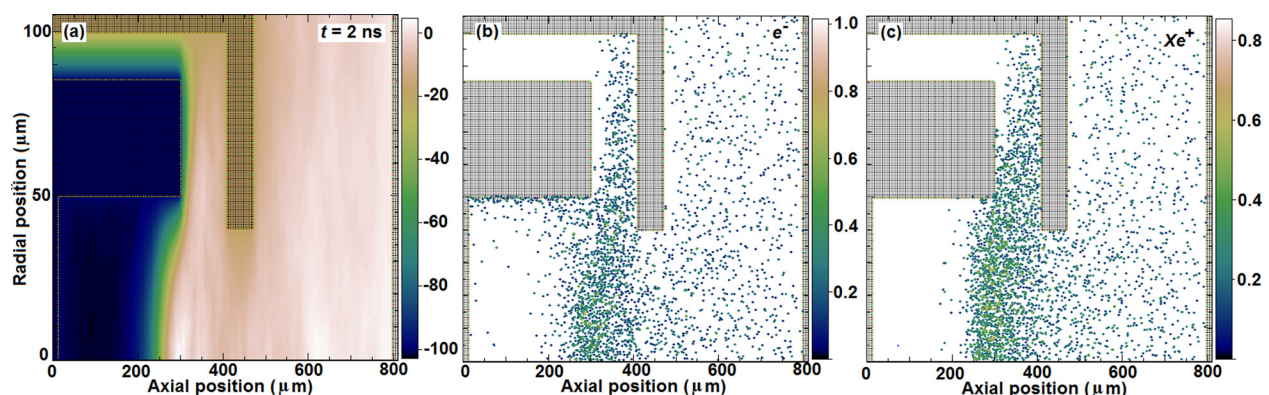


FIG. 2. Distributions of the potential (a), electron (b), and ion (c) density at $t = 2 \text{ ns}$. Plasma species densities should be multiplied by a factor of 10^{20} m^{-3} .

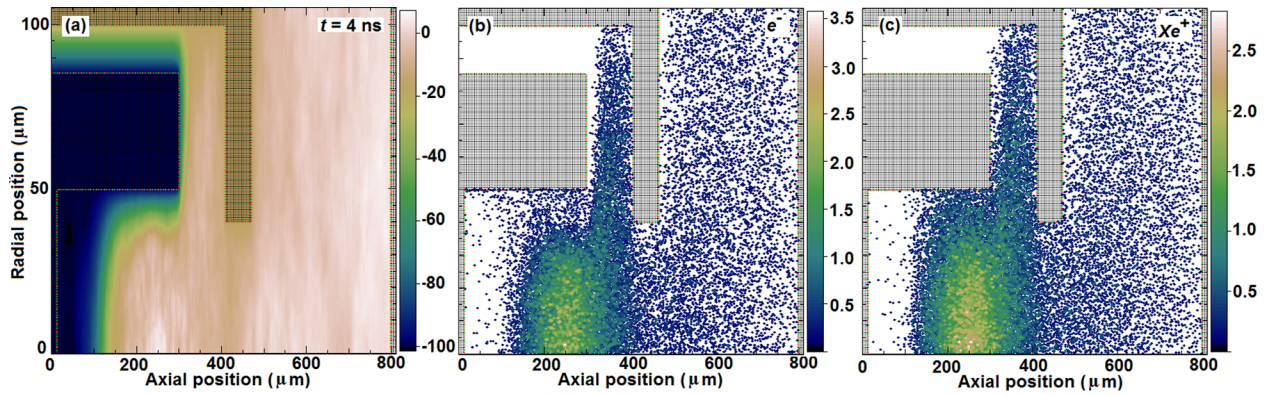


FIG. 3. Distribution of potential (a), electron (b), and ion (c) density at $t = 4$ ns. Plasma species densities should be multiplied by a factor of 10^{20} m^{-3} .

phase, the potential of the plasma with respect to the emitter increases up to ~ 90 V. Here, let us note that in commonly used HCs with significantly larger dimensions, the value of the plasma potential does not exceed 20 V.¹ This potential difference occurs mainly in the sheath having a thickness $l_s \sim 10 \mu\text{m}$, significantly smaller than the electron mean free path λ . Indeed, for electrons with an energy of 90 eV, the ionization cross section in Xe gas is $\sigma \sim 5.4 \times 10^{-20} \text{ m}^2$. Thus, the mean free path is $\lambda \sim 30 \mu\text{m}$, i.e., $\lambda \gg l_s$, and the sheath is collisionless. Moreover, the mean free path of the emitted electrons is comparable with the inner emitter radius. Thus, these electrons oscillate several times from one wall of the emitter to another in the potential well formed by the positively charged plasma before they generate new electron-ion pairs.

Let us note that emitted electrons become trapped inside the micro-HC also because of the small value of the elastic scattering cross section. The steady-state of the micro-HC operation is characterized by the formation in the keeper-anode gap of rather dense ($\sim 10^{20} \text{ m}^{-3}$) plasma generated by the electrons leaving the emitter-keeper space through the keeper's orifice [see Figs. 4(b) and 4(c)]. This plasma obtains a positive potential with respect to that formed in the emitter-keeper space and is separated from the latter by a double layer where a potential difference of ~ 10 V is realized. One can suppose that the formation of this double layer is caused by the negative potential of the keeper electrode with respect to the plasmas formed at both

its sides. This leads to ions from these plasmas being collected by the keeper, thus preventing penetration and overlapping of the plasmas and, respectively, formation of the double layer.

B. Floating keeper potential

The results of the simulations show that the micro-HC discharge when the keeper potential is turned to the floating mode at $\tau \geq 2$ ns differs from that when the keeper potential is in the constant mode. The results of the modeling for $\tau = 6$ ns are shown in Figs. 5–8. Several phases of the micro-HC operation can also be distinguished.

The first phase occurs during $t < \tau$, when the keeper potential is in the constant mode (-20 V). This phase is similar to the first two phases described in Sec. III A, namely, emitted electrons ionize the gas inside the emitter-keeper gap, and a part of these electrons penetrates the keeper's orifice and generates the plasma in the keeper-anode gap. The results of the simulations show that the density of the plasma generated outside the keeper before the floating potential of the keeper is turned on is crucial for the steady-state operation of the micro-HC, namely, the micro-HC self-sustained discharge is not realized (for the considered geometry of the micro-HC) when the keeper potential is floating, if the density of the plasma is $\leq 10^{19} \text{ m}^{-3}$ inside the keeper-anode gap.

The second phase occurs during several nanoseconds almost immediately after the floating mode of the keeper is

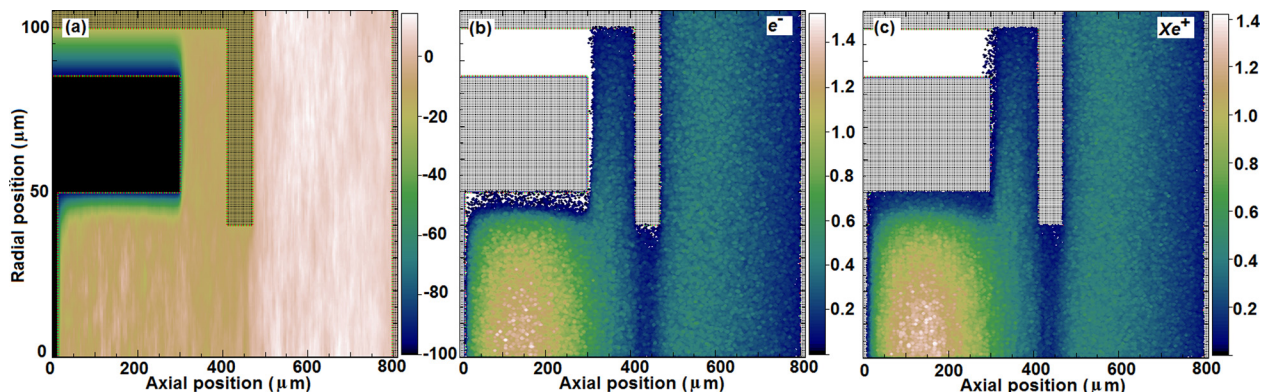


FIG. 4. Distribution of potential (a), electron (b), and ion (c) density in the steady-state phase of the micro-HC operation. Plasma species densities should be multiplied by a factor of 10^{21} m^{-3} .

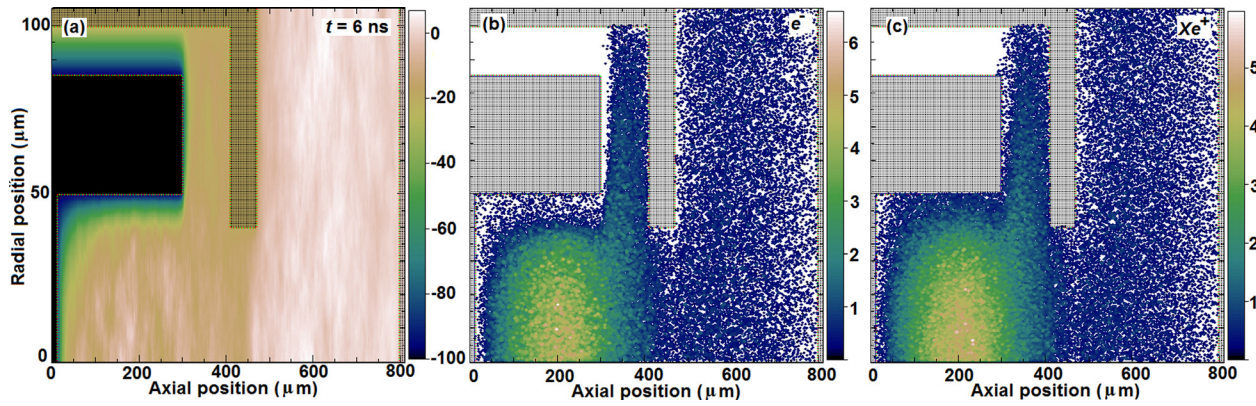


FIG. 5. Distribution of the potential (a), electron (b), and ion (c) density at $t = 6$ ns. Plasma species densities should be multiplied by a factor of 10^{20} m^{-3} .

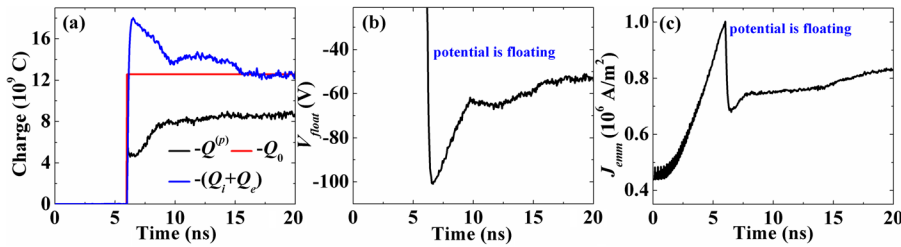


FIG. 6. Time evolution of charges (a), floating potential (b), and emission current (c) for $\tau = 6$ ns.

turned on (see Fig. 6). Figure 6(b) shows that the keeper potential acquires ~ -105 V, which slightly exceeds the value of the emitter potential. The slight excess of the keeper potential above the cathode potential can be explained by the energetic electrons appearing in the plasma due to secondary electrons generated as a result of Xe ion collisions with the emitter, the initial energy of which exceeds 5 eV. Since the absolute value of the keeper potential exceeds that of the emitter, a major part of the electrons that are emitted or are already present in the emitter-keeper space cannot leave the keeper through its orifice. At the same time, the ion flow from the plasma gradually decreases the keeper negative potential to a value that allows electron penetration through the orifice. The charging of the keeper modifies the potential distribution, leading to a decrease in the emission electron current [see Fig. 6(c)].

One can see in Fig. 5 that plasma with density $n_e \sim 10^{19} \text{ m}^{-3}$ is formed in the keeper-anode gap before the

floating mode of the keeper is turned on. The flux of the plasma ions toward the keeper partially compensates its negative charge, leading to an increase in the keeper potential [see Fig. 6(b)]. The density of electrons belonging to the plasma between the keeper and anode is sufficient to generate new electron-ion pairs (Fig. 7), maintaining the ion flux toward the keeper and neutralizing its negative charge.

The third phase (see Fig. 7) occurs when the keeper's voltage decreases to ~ -80 V. Then, the emitted electrons gain energy exceeding the ionization potential of Xe and the plasma generation by these electrons inside the emitter-keeper gap continues. The plasma formation in the emitter-keeper gap is similar to that obtained in the case of the constant keeper potential (see Sec. III A). The results of simulations show that the ion flux from the cathode-keeper plasma is not sufficient to compensate the keeper's negative charge caused by the electrons' flux. This deficit of ions is compensated by the ion flux from the keeper-anode plasma.

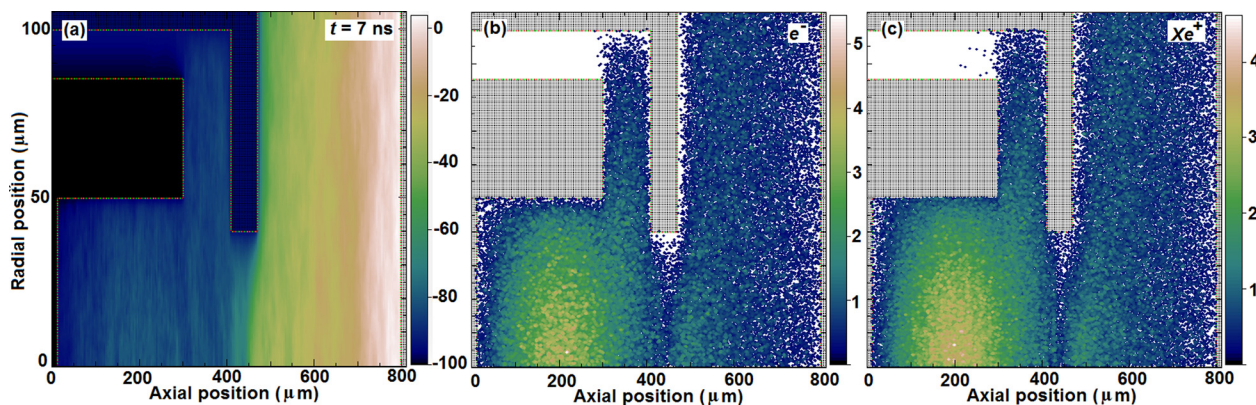


FIG. 7. Distribution of the potential (a), electron (b), and ion (c) density at $t = 7$ ns. Plasma species densities should be multiplied by the factor of 10^{20} m^{-3} .

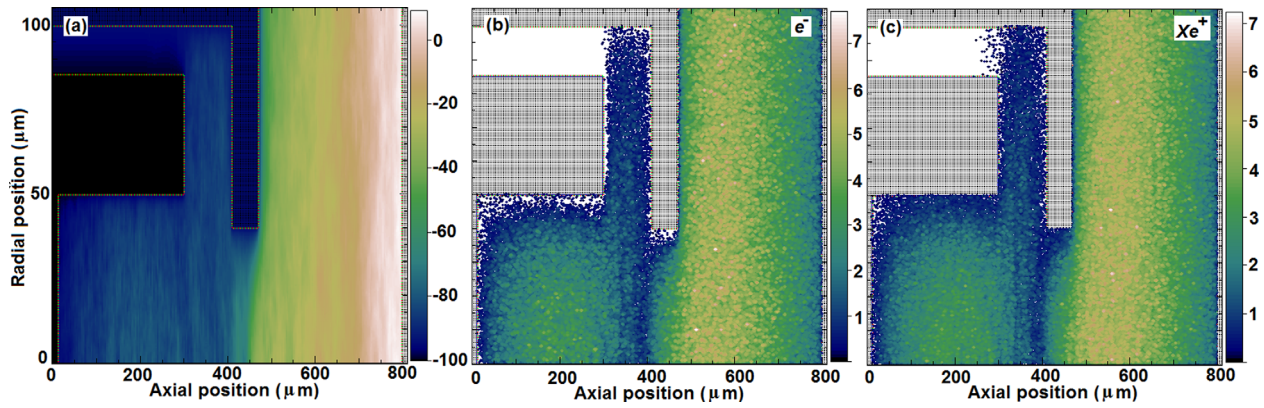


FIG. 8. Distribution of the potential (a), electron (b), and ion (c) density in the steady-state operation of the micro-HC. Plasma species densities should be multiplied by a factor of 10^{20} m^{-3} .

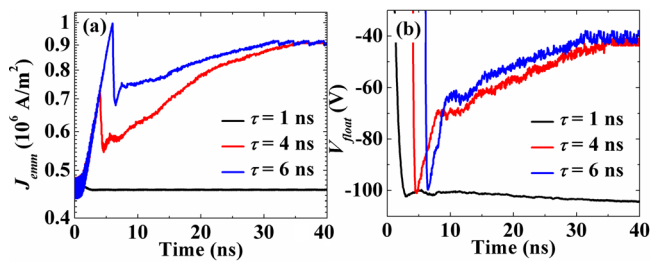


FIG. 9. Time evolution of the emission current (a) and floating potential (b) for three values of the time delay τ of the floating potential.

This means that the plasma generation in the keeper-anode gap is extremely important for the micro-HC operation when the keeper potential is floating.

It should be noted that the total charge accumulated by the keeper is constant in the steady-state regime (see Fig. 6(a), $t > 15$ ns). This indicates that the floating potential is defined correctly.

The parameters of the micro-HC steady-state operation are shown in Fig. 8. One can see that the keeper potential decreases to ~ -60 V. Similarly to the case where the keeper's potential is in constant mode, there are two plasmas separated by the double layer. However, when the keeper potential is floating the densities of these two plasmas are comparable.

Finally, in Fig. 9, one can see the dependences of the emitted current and floating potential versus the time delay τ of the turn on of the keeper's floating potential mode. One can see that at $\tau \leq 1$ ns steady-state operation of the micro-HC cannot be obtained. This is because the density of plasma electrons in the keeper-anode gap generated before the keeper's floating mode is turned on is not sufficient for continuous plasma generation. When the keeper potential obtains a

large negative value, the plasma electrons leave the keeper-anode gap without high-density plasma, and therefore, the ion flux toward the keeper is not sufficient to decrease its negative potential. At the same time, electrons from the emitter-keeper gap cannot penetrate through the orifice and support the ionization inside the keeper-anode gap. This results in decay of the plasma in the emitter-keeper space and, respectively, termination of the micro-HC operation. Let us note that at $\tau > 2$ ns, the steady-state plasma parameters do not depend on the value of τ (see Fig. 9).

C. Comparison of the two modes of micro-HC operation

To summarize, Fig. 10 shows a comparison of the plasma density, axial potential distribution, and distribution of the emitted current obtained in the steady-state operation of the micro-HC for the constant (-20 V) and floating ($\tau = 6$ ns) potential modes of the keeper.

One can see a significant difference in the parameters of the micro-HC operation for these two modes, namely, when the keeper potential is floating, the plasma densities in the emitter-keeper and keeper-anode gaps are almost equal [see Fig. 10(a)]. When the keeper's potential is constant, the plasma density in the micro-HC-keeper gap is much larger than that outside the keeper. This is explained by a significantly different potential distribution in these two micro-HC operation modes [see Fig. 10(b)]. Figure 10(b) shows that when keeper's potential is constant, the plasma potential with respect to the emitter is ~ 90 V. The axial distribution of the potential is almost uniform. In contrast, when the keeper's potential is floating, the potential gradually increases in the axial direction in both the emitter-keeper and keeper-anode gaps [Fig. 10(b)]. This means that an axial electric

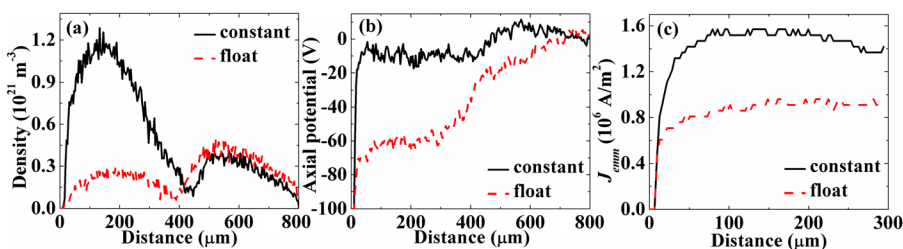


FIG. 10. Spatial distribution of plasma density (a), axial potential (b), and emitted current (c) for constant and floating keeper potential.

field exists in the plasma, because the processes inside the emitter-keeper and keeper-anode gaps cannot be considered separately. The electron fluxes exist only toward the inner surface of the keeper and anode. The ion fluxes exist toward the entire surface of the emitter and both sides of the keeper. Thus, one can consider that the total ion flux could exceed the total electron flux because of the difference in the collecting areas. In order to maintain equality between these two fluxes, the existence of an electric field inside the plasma is necessary. This electric field accelerates plasma electrons and, respectively, allows a larger amount of the electrons to overcome the sheath potential barrier, increasing the electron flux toward the inner side of the keeper.

Finally, the emitted currents, as shown in Fig. 10(c), differ significantly in these two modes. Thus, the application of the model with a constant keeper potential leads to a significant overestimation of the electron current toward the anode for the same value of the emitter temperature, as compared to that of the model with a floating keeper potential. The simulations show that the electron current density through the anode reaches $\sim 5 \times 10^6 \text{ A/m}^2$ and $\sim 1.5 \times 10^6 \text{ A/m}^2$ for the constant and floating keeper potential, respectively. It is important to note that the model with a floating keeper potential predicts a smaller ion flux and ion energy at the emitter than the model with constant keeper potential.

IV. CONCLUSION

A 2D PIC/MCC simulation of the micro-HC operation in two modes, when the potential of the keeper electrode was constant and floating, was performed. A self-consistent model of the floating keeper potential was developed. This model, which does not assume Maxwellian plasma, takes into account the charge collected by the keeper, as well as the non-compensated plasma space charge.

It is shown that the parameters of the micro-HC operation vary significantly, depending on whether the keeper potential is floating or not. When the keeper potential is constant, the density of the plasma generated inside the emitter-keeper gap is significantly larger than the density of the plasma generated inside the keeper-anode gap. When the

keeper potential is floating, the parameters of these two plasmas are almost the same. The presence of significantly dense plasma outside the keeper is crucial for the micro-HC's steady-state operation. This plasma is the main source of ion flow toward the keeper, which is necessary for neutralizing the negative charge of electron flux from the emitter-keeper gap. When such plasma is not generated prior to the time when the keeper potential is in the floating mode, the discharge in the micro-HC is not sustained. The results of the simulations show that the density and potential of the plasma formed inside the micro-HC are found to be much larger when the keeper potential is kept constant than when it is floating. This leads to artificially larger thermionic emission current density for the constant keeper's potential, which results in a larger electron current passing through the anode.

ACKNOWLEDGMENTS

The authors are grateful Dr. Irvin Haber for discussions and fruitful comments.

¹D. Goebel and I. Katz, *Fundamentals of Electric Propulsion* (John Wiley and Sons, 2008).

²E. Oks, *Plasma Cathode Electron Sources* (Wiley-VCH, 2006).

³I. G. Mikellides, D. M. Goebel, J. S. Snyder, I. Katz, and D. A. Herman, *J. Appl. Phys.* **108**, 113308 (2010).

⁴V. Vekselman, Ya. E. Krasik, S. Gleizer, V. Tz. Gurovich, A. Warshavsky, and L. Rabinovich, *J. Propul. Power* **29**, 475 (2013).

⁵D. Levko, Ya. E. Krasik, V. Vekselman, and I. Haber, *Phys. Plasmas* **20**, 083512 (2013).

⁶N. N. Koshelev and A. V. Loyan, in 30th International Electric Propulsion Conference, Florence, Italy, 17–20 Sept. 2007, IEPC-2007-103.

⁷M. Keidar, T. Zhuang, A. Shashurin, G. Teel, D. Chiu, J. Lukas, S. Haque, and L. Brieda, *Plasma Phys. Controlled Fusion* **57**, 014005 (2015).

⁸I. G. Mikellides, I. Katz, D. M. Goebel, K. K. Jameson, and J. E. Polk, *J. Propul. Power* **24**, 866 (2008).

⁹M. T. Domonkos, M. J. Patterson, and A. D. Gallimore, *J. Propul. Power* **19**, 438 (2003).

¹⁰D. P. Grote, A. Friedman, J. L. Vay, and I. Haber, *AIP Conf. Proc.* **749**, 55 (2005).

¹¹I. G. Mikellides, *Phys. Plasmas* **16**, 013501 (2009).

¹²Yu. P. Raizer, *Gas Discharge Physics* (Springer, Berlin, 1991).

¹³C. N. Dorny and B. A. Mathias, *IEEE Trans. Power Appar. Syst.* **PAS-90**, 876 (1971).